IEEE Access
Multidisciplinary ⋮ Rapid Review ⋮ Open Access Journal

Received 1 February 2024, accepted 18 April 2024, date of publication 22 April 2024, date of current version 30 April 2024.

Digital Object Identifier 10.1109/ACCESS.2024.3392295

RESEARCH ARTICLE

An Adaptive Data-Driven-Based Control for Voltage Control Loop of Grid-Forming Converters in Variable Inertia MGs

WATCHARAKORN PINTHURAT[1], (Member, IEEE), PRAYAD KONGSUK[1], TOSSAPORN SURINKAEW[2], AND BOONRUANG MARUNGSRI[3], (Member, IEEE)

[1]Department of Electrical Engineering, Rajamangala University of Technology Tawan-Ok, Chanthaburi Campus, Chanthaburi 22210, Thailand
[2]School of International and Interdisciplinary Engineering, Faculty of Engineering, King Mongkut's Institute of Technology Ladkrabang, Bangkok 10520, Thailand
[3]School of Electrical Engineering, Suranaree University of Technology, Nakhon Ratchasima 30000, Thailand

Corresponding author: Boonruang Marungsri (bmshvee@sut.ac.th)

This work was supported by Suranaree University of Technology, Thailand (Research and Development Fund), under Grant IRD7-711-66-12-41.

ABSTRACT In the transition towards sustainable energy systems, microgrid (MG) plays a pivotal role, especially in the context of variable-inertia MGs that integrate renewable energy sources (RESs) and distributed energy resources (DERs). Maintaining stable voltage control within such grids is imperative for reliable operation. This paper presents an adaptive data-driven control technique for the voltage control loop of grid-forming converters in variable-inertia MGs. The primary objective is to enhance control performance while accommodating the unpredictable nature of renewable energy sources. The approach utilizes advanced data-driven algorithms to continuously monitor and adjust control parameters based on real-time grid conditions. This adaptability allows for effective management of varying inertia and load demand, ensuring optimal grid performance. The data-driven nature of the approach enables self-adaptability, making it suitable for the dynamic MG environment. This new approach is a noteworthy advancement in controlling RESs and DERs to maintain stable voltage in MGs, without needing precise knowledge of the MG's parameters. Simulation tests and real-world examples confirm that the adaptive data-driven control method effectively optimizes voltage control in MGs with variable inertia, especially those with a high presence of RESs and DERs.

INDEX TERMS Microgrid control, voltage control, renewable energy sources, data-driven control, variable-inertia MGs, sustainable energy systems.

NOMENCLATURE

SYMBOL

$4SID$	Sub-space state-space identification.
$\hat{\boldsymbol{x}}$	Estimated state vector.
$\boldsymbol{K}$	Adaptive control matrix of voltage control loops.
$\boldsymbol{y}_i$	Output vector of the i-th SG.
$\boldsymbol{\zeta}$	Damping ratio.
ΔT_s	Stamped time of measurement.
δ	Rotor angle.
$\hat{\mathbf{x}}$	State sequences.
$\hat{A}$	Estimated state matrix.
$\hat{B}$	Input matrix.
$\hat{C}$	Output matrix.
$\hat{D}$	Feed-forward matrix.
$\hat{S}$	System matrix.
$\mathbf{H}$	Hankel matrix.
$\mathcal{O}$	Oblique projection.
ω_i	Rotor angular speed.
$\perp$	Orthogonal complement.
Θ	Extended observability matrix.
f_{4SID}	Nonlinear function of $4SID$.
H	Variable inertia.

The associate editor coordinating the review of this manuscript and approving it for publication was Ahmed Mohamed.

H_{total}	Total variable inertia.
IP, OP	Input-output pairs.
IP^*, OP^*	Specified values of input-output pairs.
k	Data index.
$K_{KE,i}$	Kinetic energy of the i-th SG.
m	Rotating mass.
M_i	Variable moment of inertia of the i-th SG.
N_b	Total number of buses.
N_i	Total number of SGs.
N_k	Total number of data within the fixed window.
N_n	RES or DER index.
N_{os}	Total number of dominant modes.
P_{DER}	Active power of DER.
P_e	Electrical power.
P_m	Mechanical power.
P_{SG}	Active power of SG.
Q_{DER}	Reactive power of DER.
Q_{SG}	Reactive power of SG.
r	Radius of the rotating part.
S	Singular value decomposition matrix.
S_{total}	Total generation capacity including SG and DERs.
t	Any given time instant.
t_1, t_2	Specific time range at a current operating point to the next operating point.
T_{window}	Window range.
V_{DER}	Bus voltage of DER.
V_{int}	Internal voltage.
V_{SG}	Bus voltage of SG.
W_1,W_2	Weighting factors.
X	Reactance.

ABBREVIATION

BPC	Bidirectional power converter.
CPP	Conventional power plant.
DER	Distributed energy resource.
ESS	Energy storage system.
GFL	Grid-following converter.
GFM	Grid-forming converter.
MG	Microgrid.
PV	Photovoltaic.
RoCoV	Rate of change of voltage.
RES	Renewable energy source.
SG	Synchronous generator.
WG	Wind generator.

I. INTRODUCTION

A. A SIGNIFICANCE AND PROBLEM

The development and integration of renewable energy sources (RESs) into modern power systems have revolutionized the landscape of energy generation and distribution [1]. Microgrids (MGs), in particular, have emerged as a promising solution for enhancing the resiliency and sustainability of electrical grids [2], [3]. Moreover, the inherent variability and uncertainty associated with RESs in variable inertia MGs demand novel control strategies capable of dynamically adapting to changing operating conditions [4], [5], [6]. The existing control techniques often struggle to effectively address these issues, resulting in voltage deviations, harmonic distortions, potential grid instability, etc [7]. However, in the context of variable inertia MGs, which may comprise a mix of different energy sources and energy storage systems, the control of grid-forming converters has become a complex and critical challenge. Ensuring voltage control in these systems is of paramount importance for maintaining MG stability and reliability.

An adaptive data-driven control is crucial in variable inertia MGs due to the introduction of RESs and distributed energy resources (DERs). RESs and DERs are vital for sustainable energy, but they are unpredictable and bring uncertainties to the power system [8]. These uncertainties challenge the conventional control techniques, which necessitate innovative solutions that can adapt to ever-changing operating conditions. In variable inertia MGs, which often feature a blend of RESs and DERs and storage systems, ensuring reliable voltage control is paramount. Robust data-driven control techniques can effectively address the dynamic and complex nature of these systems. They can continuously monitor real-time data, such as energy generation and load demand, and adapt the control strategy accordingly. This adaptability is crucial for maintaining grid stability, as it mitigates voltage deviations, harmonic distortions, and the potential for grid instability. Furthermore, robust data-driven control contributes to the resilience and sustainability of MGs. By reducing the risk of voltage deviations and power quality issues, it enhances grid reliability. This adaptability also supports the seamless integration of renewable energy sources, improving energy efficiency and reducing greenhouse gas emissions. As a result, robust data-driven control plays a vital role in ensuring the stability, efficiency, and sustainability of MG systems, making them a more reliable and environmentally friendly component of the broader electrical grid.

B. RELATED PUBLICATIONS

Previously, there are several research works deal with the problems of low-inertia systems and MGs. In [9], the authors introduce a proposed virtual synchronous control technique for mitigating wideband oscillations in a DC MG by emulating inertia and damping. This study explores the relationship between rate of change of voltage (RoCoV), DC voltage nadir, damping, inertia, and wideband oscillation and offers a unified concept connecting oscillation-related stability to transient responses. Theoretical results are compared with simulations and experiments to validate the proposed approach. In [10], the authors present a novel distributed control method that enhances the inertia of MGs by utilizing rate of change of frequency (RoCoF) and RoCoV to quantify frequency and voltage inertia. The method includes a fully distributed algorithm with constrained changing rates, which effectively utilizes distributed generation power reserves to

enhance MG inertia. It outperforms conventional distributed control methods under disturbances and delays, and its effectiveness is demonstrated through MATLAB simulations and a hardware experiment. In [11], a virtual inertia and damping control strategy for bidirectional DC converters in a DC MG is introduced. The virtual inertia and damping control emulates inertia using energy storage systems (ESSs) and incorporates damping to damp voltage oscillations. The control approach enables multi-parallel ESS operation with droop control and optimizes parameters for improved voltage stability in islanded DC MGs. Simulation results confirm the effectiveness of ESS acting as synthetic inertia, leading to better control performance compared to other methods. In [12], this study addresses the power quality issues in hybrid AC/DC microgrids with low inertia due to renewable energy integration. It presents an adjustable inertia implementation method using a two-stage bidirectional power converter (BPC). The first stage emulates a virtual synchronous generator to support the AC subgrid/subMGs and enhance AC bus frequency response, while the second stage controls the BPC's built-in capacitor to provide adjustable inertia for the DC subgrid and improve DC bus voltage response. Small-signal analysis confirms the stability of the proposed approach, and experimental results on a real-time hardware-in-loop platform demonstrate its effectiveness. In [13], the authors discuss DC microgrid voltage oscillations caused by negative damping, power converter-network interaction, and positive feedback. It establishes a relationship between DC current and voltage and proposes a virtual inertia control strategy to improve damping and create negative feedback. Experimental validation is performed using StarSim hardware-in-the-loop experiments.

In [14], a novel virtual inertia control method for addressing the low inertia issue in power-converter-interfaced MGs is presented. It utilizes a feed-forward decoupling strategy to eliminate coupling between active and reactive power, allowing for increased inertia in the MG. Small-signal modeling, parameter analysis, and simulation studies confirm the effectiveness of this control strategy, which can enhance MG inertia and power quality. In [15], the authors introduce a cascaded buck-boost converter as a high-power-density and efficient alternative for ESSs in DC MGs. A virtual DC machine control strategy is proposed to enhance DC bus voltage stability by charging and discharging the ESS through the converter, and it includes a first-order inertia loop. Simulations in Matlab/Simulink demonstrate the stability of this approach under various scenarios, supported by small-signal analysis. In [16], an iterative approach to fine-tune control parameters for multiple power converters in an MG operating in both grid-connected and grid-islanded modes, is presented. The approach employs an optimization-based strategy and utilizes local measurements along with previous iteration results to determine optimal control parameters. The proposed method effectively improves MG control performance, simplifying the tuning process, and can be applied to complex MGs without requiring a detailed model of the MG itself. Validation results from the CIGRE LV benchmark microgrid show that the approach ensures reliable performance in various operational modes, with deviations from rated frequency within 2.2% during faults and below 0.3% in grid-islanded or grid-connected scenarios. Also in [17], this work introduces an efficient control strategy for power management, voltage balancing, and grid synchronization in a DERs-based MG. The control scheme, developed and tested in a real-time digital simulator, ensures stability and reliability in grid-connected and islanded operation modes under high penetration of DERs. It includes a controller for the diesel generator to maintain MG frequency during islanded mode and switched capacitor banks for voltage balancing during grid synchronization. The proposed approach proves effective in real-time simulations and offers potential applications for complete MG operation control. In [18], the authors introduce a two-level control scheme for DC MGs, designed to ensure accurate power sharing and voltage regulation during islanded operation. In the primary control level, a $P - V$ droop method eliminates power sharing dependency on line resistances, and a voltage derivative restoration mechanism in the secondary level enhances voltage stability. Small-signal stability analysis and real-time simulations validate the effectiveness of the proposed approach, which improves upon conventional methods.

However, the research gaps remain as follows: (i) The contributions of previous works highlight the importance of adaptive data-driven control in variable inertia MGs but does not explicitly address the specific challenges, techniques, or methodologies for implementing such controls. This presents a gap in the literature regarding the detailed development and practical implementation of robust data-driven control strategies for variable inertia MGs; (ii) While the they mention that the proposed approach does not require exact MG parameters, it does not provide a clear methodology or technique for achieving parameter-free controller design. This gap lies in the need for more concrete guidance on how to design controllers without detailed system parameters, especially in the context of variable inertia MGs; (iii) The papers emphasize the improved integration of RESs and DERs facilitated by the proposed technique. However, it lacks a detailed exploration of the challenges and methods for seamlessly integrating RESs and DERs into variable inertia MGs. This gap could be addressed by providing insights into RES integration strategies and their impacts on energy efficiency and emissions reduction; (iv) While the mentioned research works address control strategies for MGs and low-inertia systems, there is a research gap in the development of adaptive control techniques specifically designed for GFM converters. Future researches could focus on creating adaptive control methods that can efficiently manage voltage stability and power quality by dynamically adjusting control parameters based on real-time conditions

and system requirements. This would help GFM converters better respond to variable MG conditions and enhance overall performance and stability.

C. SUMMARY OF KEY CONTRIBUTIONS

To address these problem in the literature, this paper addresses the significant issue of voltage control within variable inertia MGs and proposes an innovative, adaptive data-driven-based control technique to overcome the associated challenges. The major contributions of our paper are threefold as follows:

- We present an adaptive control technique specifically tailored for GFM converters used in RESs and DERs within variable inertia MGs. Our proposed technique eliminates the need for precise knowledge of the MG's parameters when designing controllers. Furthermore, it enhances grid stability in variable inertia MGs by delivering adaptive voltage control capable of effectively responding to fluctuations in power generation and load demand. This proposed strategy, in turn, can effectively reduce the risk of voltage deviations and grid instability.
- This innovative approach contributes to the overall resilience and reliability of MG systems by allowing for the seamless integration of various energy sources, RESs, and DERs, and adapting to changing operating conditions, ensuring continuous and reliable energy supply. To minimize interference with active power flow, we employ reactive power to stabilize both voltages and their fluctuations.
- The simulation results have been validated within an LV MG that incorporates RESs and DERs under a range of MG and operating conditions. To the best of our knowledge, this marks the initial endeavor to introduce an adaptive data-driven control technique for the voltage control loop of grid-forming converters in variable inertia MGs.

D. PAPER ORGANIZATION

The remaining sections of this paper are structured as follows: In Section II, we provide an overview of the fundamental principles and motivations behind adaptive data-driven-based control techniques. We outline the scope of our study and the specific objectives we aim to achieve through our research. In Section III, this section presents the details of the adaptive data-driven voltage control strategy we have developed. We discuss the methodology, algorithms, and data sources used in the creation of this control strategy. After that Section IV presents the results of numerical simulations and analyses based on the adaptive data-driven voltage control strategy. We discuss the performance, efficiency, and effectiveness of the proposed technique, supported by quantitative data and in-depth discussions. Finally, Section V summarizes the significant findings and contributions of our research. In this section, moreover, we draw conclusions from the obtained results and discuss their implications.

II. OVERVIEW OF VARIABLE INERTIA MG AND ADAPTIVE DATA-DRIVEN-BASED CONTROL

A. VARIABLE INERTIA MG

In a conventional power system, the majority of electricity is generated from sources such as coal, nuclear, and hydroelectric power. One crucial aspect of this system lies in the kinetic energy stored within the rotating components of the synchronous generator (SG), which plays a pivotal role in managing frequency dynamics and ensuring stability. The inherent contribution of inertia serves as an indispensable feature of the SG. During instances of power imbalances, such as variations in load/generation or grid faults, the synchronous generator adapts its rotational speed, relying on both rotor inertia and controller actions. Through this intricate process, the SG upholds synchronism, acting as a safeguard against grid collapse or blackout scenarios. The rotating mass of the generator becomes a dynamic contributor of kinetic energy to the grid, either supplying or absorbing it in response to frequency fluctuations. This intricate interplay of components underscores the resilience and reliability of the power system in navigating diverse operational challenges [19], [20].

In the face of this challenge, the SG's role becomes even more critical [19], [20]. Its ability to alter rotational speed based on both rotor inertia and advanced controller actions becomes a linchpin in maintaining grid stability among the variable and intermittent nature of renewable energy inputs. This adaptive capacity ensures that the power system remains resilient, effectively mitigating the impact of load/generation variations and grid faults. Furthermore, as we delve deeper into the dynamics of future power grids/MGs, the SG's contribution extends beyond preventing grid collapse [19], [20]. The evolving landscape demands a more nuanced understanding of how the rotating mass of the generator interacts with the grid under dynamic variations. This intricate interplay not only contributes kinetic energy to the grids/MGs but also actively participates in the absorption or release of energy, aligning with the ever-changing requirements of a modern, sustainable power ecosystem [21].

Here, in a low-inertia MG, the moment of inertia of the i-th SG (denoted by M_i) is given in the form,

$$M_i = \int_{t_1}^{t_2} r_i^2 \mathrm{d}m_i = r_i^2 m_i, \tag{1}$$

where t_1 and t_2 are the specific time range at a current operating point to the next operating point, r is the radius of the rotating part of an SG in m, and m is the mass in kg.

Let ω_i is the i-th SG's rotor angular speed, from (1), the kinetic energy of the i-th SG (denoted by $E_{KE,i}$) associated to J_i can be expressed as,

$$K_{KE,i}(t) = \frac{1}{2} M_i \omega_i^2(t). \tag{2}$$

Next, the swing equation of a MG can be expressed as the dynamic evolution of E_{KE} within the system,

which effectively captures the interplay between changes in mechanical power and electrical power, as in the form,

$$\frac{\mathrm{d}K_{KE,i}(t)}{\mathrm{d}t} = \frac{1}{2}\frac{\mathrm{d}}{\mathrm{d}t}\left(M_i\omega_i^2(t)\right) = P_{m,i}(t) - P_{e,i}(t), \quad (3)$$

where P_m and P_e are the mechanical and electrical powers, respectively.

The bus voltage variation in a MG can be influenced by the inertia present in the system as inertia is a measure of a system's resistance to changes in speed or rotational motion [22]. In traditional power systems with high-inertia generators, the impact of sudden changes in load or generation is often mitigated due to the inherent stability provided by the rotating masses [22]. However, in low-inertia MGs with a significant presence of DERs, this scenario changes. The swing equation is typically derived from the mechanical power balance in a SG. The mechanical power ($P_{m,i}$) supplied to the generator is equal to the rate of change of kinetic energy $\frac{\mathrm{d}E_{KE,i}}{\mathrm{d}t}$ of the rotating masses in the system.

Taking the derivative of kinetic energy with respect to time gives the rate of change of kinetic energy,

$$\frac{\mathrm{d}E_{KE,i}(t)}{\mathrm{d}t} = M_i\frac{\mathrm{d}^2\omega_i(t)}{\mathrm{d}t^2}. \quad (4)$$

Substituting (4) back into the power balance equation (3), we have,

$$P_{m,i}(t) - P_{e,i}(t) = P_{SG,i}(t) = M_i\frac{\mathrm{d}^2\omega_i(t)}{\mathrm{d}t^2}. \quad (5)$$

Now, electrical power ($P_{SG,i}$) generated by an SG is given by,

$$P_{SG,i}(t) = \frac{V_{int,i}(t)V_i(t)}{X}\sin(\delta(t)), \quad (6)$$

where V_{int} is the internal voltage, X is the reactance, and δ is the rotor angle.

Equating the mechanical power to the electrical power, we arrive at the i-th voltage related to the swing equation,

$$V_i(t) = \frac{M_i\frac{\mathrm{d}^2\omega_i(t)}{\mathrm{d}t^2}X_i}{V_{int,i}}. \quad (7)$$

In (7), this equation represents the dynamic behavior of an SG in a low-inertia MG and is known as the swing equation or we can write $V_i(t) = f(M_i)$, where f is the nonlinear function. It describes the relationship between changes in mechanical power, angular velocity, and electrical power in the system. This equation signifies the balance between the mechanical power ($M_i \cdot \omega(t) \cdot \frac{\mathrm{d}\omega_i(t)}{\mathrm{d}t}$), related to the kinetic energy and rotational motion of the system, and the electrical power generated by the synchronous generator. In practical terms, changes in angular velocity ($\frac{\mathrm{d}\omega_i(t)}{\mathrm{d}t}$) on the left side of the equation indicate the system's response to disturbances or alterations in mechanical or electrical conditions.

Referring to (4), when the grid's inertia varies over time, (4) can be expressed as $\frac{\mathrm{d}E_{KE,i}(t)}{\mathrm{d}t}$. Consequently, the inertia $H_i(t)$ is no longer constant and can be represented in the time domain as,

$$H_i(t) = \frac{E_{KE,i}(t)}{S_{SG,i}(t)} = \frac{M_i\omega_i^2(t)}{2S_{SG,i}(t)}. \quad (8)$$

The variable inertia $H_i(t)$ is defined as the time period, expressed in seconds, during which the system can consistently generate the nominal power solely relying on the kinetic energy stored within the rotating mass, as illustrated in equation (8) [23]. Consequently, the total variable inertia $H_{tota}(t)$ is expressed by,

$$H_{total}(t) = \frac{\sum_{i=1}^{N_i} M_iS_i(t)}{S_{total}(t)} = \frac{\sum_{i=1}^{N_i} E_{KE,i}(t)}{S_{total}(t)}, \quad (9)$$

where N_i is the total number of SGs, and S_{total} is the total generation capacity including SG and DERs.

Considering (9), when the DERs penetrate to the MG while the term $\sum_{i=1}^{N_i} M_iS_i(t)$ is constant. Accordingly, this scenario increases $S_{total}(t)$ and subsequently decreases $H_{total}(t)$. As $H_{total}(t)$ decreases due to higher DER penetration, a reduction in total inertia can amplify voltage fluctuations within the MG, rendering it more susceptible to variations in RES output. Furthermore, lower total inertia leads to faster MG dynamics, enabling swift adjustments to changes in load or generation. This heightened responsiveness can affect the overall stability and efficiency of the MG.

B. OVERVIEW OF ADAPTIVE DATA-DRIVEN-BASED CONTROL

Fig. 1 demonstrates the overview of MG with adaptive data-driven-based control. We assume the existence of a total of N_j MGs. Each MG comprises distributed loads, DERs, and conventional generators with inertia support—such as distributed/aggregate diesel generators or synchronous generators. These MGs are interconnected, and additional MGs, as well as the remainder of the network, may be connected subsequently.

On one hand, the problem stems from the inherent challenges in obtaining precise parameters for MG components, particularly DERs, owing to their intermittent natures. The fluctuating and unpredictable behavior of RESs makes it difficult to ascertain the exact characteristics of these systems. Consequently, this uncertainty poses a significant obstacle when trying to comprehensively investigate the state of the system and design an effective controller. To address this issue, a data-driven-based method becomes necessary. Instead of relying on predetermined or assumed parameters, this approach involves utilizing real-world data and observations to inform the modeling and control strategies. By leveraging data-driven techniques, such as machine learning algorithms or statistical methods, the system can adapt to the dynamic and uncertain nature of MGs and DERs. This allows for a more flexible and robust control approach, enhancing the overall performance and resilience of the system in the face of variable and unpredictable conditions.

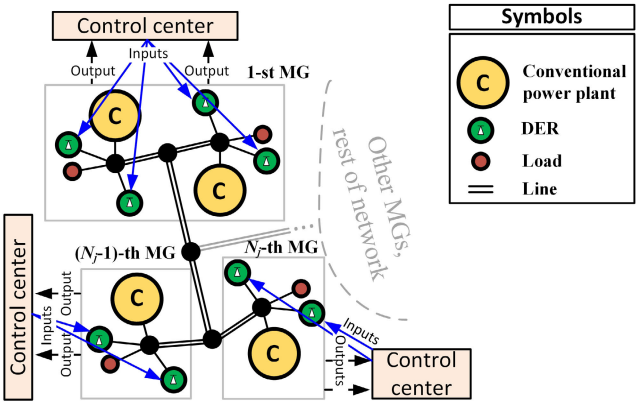

FIGURE 1. Overview of MG and control strategy.

Here, at any given time t, we gather the output vector (i.e., $\boldsymbol{y}$) from the respective MG as,

$$\boldsymbol{y}(t) = \left[\boldsymbol{y}_1(t), \boldsymbol{y}_2(t), \boldsymbol{y}_3(t), \ldots, \boldsymbol{y}_{N_j}(t)\right]. \tag{10}$$

Here, we consider the impacts of measurement. We assume that the stamped time of measurement is ΔT_s. Within a fixed window of T_{window}, let $k = 1 \cdot \Delta T_s, \ldots, N_k \cdot \Delta T_s$ represent the data index, where N_k is the total number of data within the fixed window and $T_{window} = N_k \Delta T_s$ is the window range. Note that the discrete representation of $\boldsymbol{y}(t)$ at any given t, denoted as $\boldsymbol{y}[t+k]$ when $\boldsymbol{y}[t+k]$ is defined with respect to the values of $\boldsymbol{y}$ at time $t+k$, we have,

$$\begin{aligned}\boldsymbol{y}[t+k] = [&\boldsymbol{y}[t+1\Delta T_s], \boldsymbol{y}[t+2\Delta T_s], \boldsymbol{y}[t+3\Delta T_s], \\ &\ldots, \boldsymbol{y}[t+N_k\Delta T_s]], \boldsymbol{y}[k] \in \left\{\boldsymbol{y}_1[k], \ldots, \boldsymbol{y}_{N_j}[k]\right\}.\end{aligned} \tag{11}$$

We collect the data of all generations including SG, RESs, and DERs. Let $n = 1, 2, 3 \ldots, N_n$ is the RES or DER index and N_n is the total number of RESs and DERs in i-th MG, each vector encompasses the voltage values of all buses ($V_{SG,i}(t)$, $V_{DER,n}(t)$), the active powers of all buses ($P_{SG,i}(t)$, $P_{DER,n}(t)$), and the reactive powers of all buses ($Q_{SG,i}(t)$, $Q_{DER,n}(t)$). In the moving window with variable inertia, the representation of these variables in the form of (11) can be expressed as,

$$\begin{aligned}&V_{SG,i}[t+k] \\ &= \left[V_{SG,i}[t+\Delta T_s], \ldots, V_{SG,i}[t+N_k\Delta T_s]\right], \\ &V_{DER,n}[t+k] \\ &= \left[V_{DER,n}[t+\Delta T_s], \ldots, V_{DER,n}[t+N_k\Delta T_s]\right], \\ &P_{SG,i}[t+k] \\ &= \left[P_{SG,i}[t+\Delta T_s], \ldots, P_{SG,i}[t+N_k\Delta T_s]\right], \\ &P_{DER,n}[t+k] \\ &= \left[P_{DER,n}[t+\Delta T_s], \ldots, P_{DER,n}[t+N_k\Delta T_s]\right], \\ &Q_{SG,i}[t+k] \\ &= \left[Q_{SG,i}[t+\Delta T_s], \ldots, Q_{SG,i}[t+N_k\Delta T_s]\right], \\ &Q_{DER,n}[t+k] \\ &= \left[Q_{DER,n}[t+\Delta T_s], \ldots, Q_{DER,n}[t+N_k\Delta T_s]\right].\end{aligned} \tag{12}$$

Utilizing the formulations provided in (12), we employ a data-driven approach to identify the MG models including SGs, RESs, and DERs. The next section will provide a detailed explanation of the proposed adaptive data-driven approach, specifically focusing on the design of adaptive controllers for voltage control loops of controllable distributed energy resources. Notably, this approach relies solely on the variables $V_{SG,i}[t+k]$, $V_{DER,n}[t+k]$, $P_{SG,i}[t+k]$, $P_{DER,n}[t+k]$, $Q_{SG,i}[t+k]$, and $Q_{DER,n}[t+k]$ obtained from measurements in the MG. Here, it is assumed that the measurements are ideal without communication issues.

III. PROPOSED ADAPTIVE DATA-DRIVEN VOLTAGE CONTROL DESIGN

A. MG IDENTIFICATION USING 4SID

MG identification using the sub-space state-space identification (known as 4*SID*) employs the fourth-order 4*SID* method to extract dynamic models from input-output data. Its advantage lies in accurately capturing the complex dynamics of MGs with DERs [6]. It accurately determines a system's dynamic model without needing precise parameters. By analyzing input-output data, it identifies the system's state-space representation, allowing for effective modeling and control without explicit parameter knowledge. This method is particularly useful in scenarios where obtaining exact system parameters is challenging or impractical [6]. Besides, the 4*SID* method efficiently handles multivariate time-series data, enabling precise modeling of MG components' interactions. This approach is particularly beneficial for adaptive control and optimization strategies in MGs with DERs, enhancing grid resilience and efficiency by accommodating diverse and changing energy sources within the MG [24], [25].

After obtaining the MG outputs in the form given by Equation (12), we define $IP[k]$ and $OP[k]$ as the input-output pairs utilized for subspace state-space identification using the (4*SID*) method and $\left\{V_{SG,i}[k], \ldots, Q_{DER,n}[k]\right\} \in \{IP[k], OP[k]\}$. Subsequently, we proceed to identify the system matrices and associated indices through the following steps:

1) Equally partition the measured signals $IP[k]$ and $OP[k]$;
2) Let define the oblique projection $\mathcal{O}$,

$$\begin{aligned}\mathcal{O}[k-1] &= OP[k-1]/_{IP[k-1]}\mathbf{H}[k+1], \\ &= \Theta[k-1]\hat{\boldsymbol{x}}[k+1],\end{aligned} \tag{13}$$

where $\mathbf{H}$ is the Hankel matrix containing the past inputs and outputs, $\hat{\boldsymbol{x}}$ is the estimated state matrix, and Θ is the extended observability matrix;
3) Compute the oblique projections at patterns k and $k-1$ using the expressions: $\mathcal{O}[k] = \frac{OP[k]}{IP[k]}\mathbf{H}[k]$, and $\mathcal{O}[k-1]$ as defined in (13);

4) Calculate the singular value decomposition (known as *SVD*) and determine the estimated model ordered by inspecting the singular values in $S[k] = \begin{bmatrix} S_{11}[k] & 0 \\ 0 & 0 \end{bmatrix}$. Next, partition the *SVD* to obtain $U_1[k]$ and $S_{11}[k]$ by,

$$\begin{aligned} &W_1[k]\mathcal{O}[k]W_2[k] \\ &= [U_1[k]\ U_2[k]] \begin{bmatrix} S_{11}[k] & 0 \\ 0 & 0 \end{bmatrix} \begin{bmatrix} V_1^\top[k] \\ V_2^\top[k] \end{bmatrix}, \\ &= U_1[k]S_{11}[k]V_2[k]^\top, \end{aligned} \tag{14}$$

where $W_1 = [U_1\ U_2]$ and $W_1 = [V_1^\top\ V_2^\top]^\top$ are the weighting matrices;

5) Determine $\Theta[k]$ and $\Theta[k-1]$ as,

$$\Theta[k] = W_1^{-1}[k]U_1[k]\sqrt{S_{11}[k]}, \tag{15}$$

$$\Theta[k-1] = \underline{\Theta}[k], \tag{16}$$

where $\underline{\Theta}[k]$ means the matrix $\Theta[k]$ without the last row;

6) The state sequences $\hat{\mathbf{x}}[k]$ and $\hat{\mathbf{x}}[k+1]$ are computed through the following calculations,

$$\hat{\mathbf{x}}[k] = \Theta[k]^\perp \mathcal{O}[k], \tag{17}$$

$$\hat{\mathbf{x}}[k+1] = \underline{\Theta^\perp}[k]\mathcal{O}[k-1], \tag{18}$$

where superscript $\perp$ means the orthogonal complement;

7) Solve the set of estimated state matrix $\hat{A}$, input matrix $\hat{B}$, output matrix $\hat{C}$, and feed-forward matrix $\hat{D}$ by

$$\begin{bmatrix} \hat{\mathbf{x}}[k+1] \\ OP^*[k] \end{bmatrix} = \begin{bmatrix} \hat{A}[k] & \hat{B}[k] \\ \hat{C}[k] & \hat{D}[k] \end{bmatrix} \begin{bmatrix} \hat{\mathbf{x}}[k] \\ IP^*[k] \end{bmatrix}, \tag{19}$$

where $IP^*[k]$ and $OP^*[k]$ represent the specified values of $IP[k]$ and $OP[k]$ at any given sequence k, respectively. It is important to note that this set of matrices can be determined through the application of a linear least squares method.

8) Repeat steps 1) to 7) for $t+k = t+\Delta T_s, \ldots, t+N_k\Delta T_s$. This yields matrices $[\hat{A}[t+\Delta T_s], \cdots, \hat{A}[t+N_k\Delta T_s]]$, $[\hat{B}[t+\Delta T_s], \cdots, \hat{B}[t+N_k\Delta T_s]]$, $[\hat{C}[t+\Delta T_s], \cdots, \hat{C}[t+N_k\Delta T_s]]$, and $[\hat{D}[t+\Delta T_s], \cdots, \hat{D}[t+N_k\Delta T_s]]$. Subsequently, stability indices can be derived for each moving window, providing valuable information for controller design;

9) Substitute $k = t+k$ and compute the 4*SID* of the MG at any time instant k in Fig. 1,

$$\begin{aligned} &f_{4SID}(IP[t+k], OP[t+k]) \\ &= \left[\hat{A}[t+k], \hat{B}[t+k], \hat{C}[t+k], \hat{D}[t+k]\right], \end{aligned} \tag{20}$$

where f_{4SID} is the nonlinear function of 4*SID* conducted by steps 1) to 8).

B. DESIGN OF ADAPTIVE CONTROLLER

Designing an adaptive controller through a data-driven approach at each k-th MG operating point facilitates up-to-date adjustments based on observed MG behavior. This approach enhances adaptability to dynamic conditions, ensuring optimal performance and stability across various operational states within the MG system. In this paper, our objective is to improve the damping characteristics of the dominant modes in the MG induced by RES and DER. After obtaining $\bar{A}[t+k]$, $\bar{B}[t+k]$, $\bar{C}[t+k]$, and $\bar{D}[t+k]$, the system matrix at $t+k$ (denoted by $\hat{G}[t+k]$) can be derived as,

$$\hat{G}[t+k] = \begin{bmatrix} \hat{A}[t+k] & \hat{B}[t+k] \\ \hat{C}[t+k] & \hat{D}[t+k] \end{bmatrix}. \tag{21}$$

Damping ratio of (21) ($\boldsymbol{\zeta}[t+k]$) can be calculated by,

$$\begin{aligned} &\det(\hat{A}[t+k] - \boldsymbol{\zeta}[t+k]I) = 0, \\ &\boldsymbol{\zeta}[t+k] = \left[\zeta_1[t+k], \ldots, \zeta_{N_{os}}[t+k]\right], \end{aligned} \tag{22}$$

where I is the identify matrix and N_{os} is the total number of dominant modes.

The first objective, denoted as $\boldsymbol{J}_1$, is to maximize the values of $\boldsymbol{\zeta}[t+k]$ to exceed 3%. This objective is formulated as,

$$\begin{aligned} &\max(\boldsymbol{J}_1[t+k]) = \max(\boldsymbol{\zeta}[t+k]), \\ &s.t.\ :\ \forall \boldsymbol{\zeta}[t+k] \geq 0.03. \end{aligned} \tag{23}$$

To enhance voltage control capability, the range of voltage changes (defined as (*RoCoV*)) for all generators' buses is considered and constrained within an acceptable range. Consequently, the second objective ($\boldsymbol{J}_2$) aims to improve the $RoCoV[t+k]$ as,

$$\begin{aligned} &\min(\boldsymbol{J_2}[t+k]) = \min(RoCoV[t+k]), \\ &RoCoV[t+k] = \sum_{i=1}^{N_i} |V_{SG,i}[t+k] - V^*_{SG,i}| \\ &\qquad + \sum_{n=1}^{N_n} |V_{DER,n}[t+k] - V^*_{DER,n}|. \end{aligned} \tag{24}$$

Accordingly the objective to design the controller is,

$$\min(W_1\boldsymbol{J}_1^{-1}[t+k] + W_2\boldsymbol{J}_2[t+k]), \tag{25}$$

where W_1 and W_2 are the weighting factors for the first and second terms of (25), respectively.

At an operating point, after optimizing the control parameters using (25), the control matrix $\boldsymbol{K}$ can be represented in the transfer function form and is reduced to a practical 2nd-order by [26],

$$\begin{aligned} &\boldsymbol{K}[t+k] \\ &= \frac{b[t+k]\left(a_0[t+k] + a_1[t+k]s + a_2[t+k]s^2\right)}{c_0 + c_1[t+k]s + c_2[t+k]s^2}, \end{aligned} \tag{26}$$

where s is the complex frequency variable, and b, a_0, a_1, a_2, c_0, c_1, and c_2 are the variable control parameters which may be changed according to MG operating point or if (i) the conditions specified in (23) are not satisfied, or (ii) the MG topology changes.

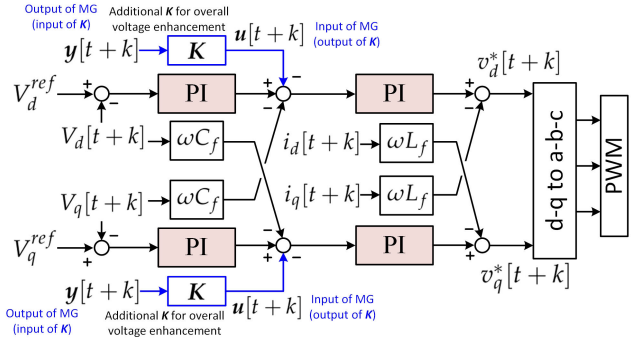

FIGURE 2. GFM control strategy with additional signals from K for overall voltage enhancement.

C. PROPOSED GRID-FORMING CONVERTER CONTROL FOR OVERALL VOLTAGE ENHANCEMENT

Voltage control loops in GFM converters for low-inertia MGs with DERs are essential for maintaining voltage stability, supporting frequency regulation, enabling grid-forming operation, detecting islanding events, and enhancing the overall resilience of the MG. To regulate the voltage, the input $\boldsymbol{u}[t+k]$ is introduced into the voltage control loop of the GFM converters, as illustrated in Fig. 2, where subscripts dq represents the direct and quadrature axes. In this design concept, two main control loops exist: the inner voltage control loop and the inner current control loop. The inner voltage control loop focuses on regulating the output voltage of the GFM converter, while the inner current control loop is responsible for controlling the current. Both loops play essential roles in ensuring the stability, reliability, and efficient operation of the MG by responding to changes in load, disturbances, and variations in the connected DERs. These control loops are primarily responsible for maintaining the bus voltage, offering a rapid response to uncertainties within the MG and the intermittent nature of DERs. Moreover, integrating feed-forward terms in both loops, the terms such as $-V_d[t+k]\omega C_f$, $-V_q[t+k]\omega C_f$, $-i_d[t+k]\omega L_f$, and $-i_q[t+k]\omega L_f$, at the summation point in voltage and frequency control loops of DER converters within MG control yields multiple advantages. These additions enable the system to anticipate and counteract disturbances before they affect the output. By incorporating potential variations in load or renewable energy sources, the feed-forward terms enhances transient response and minimizes deviations in voltage and frequency. These proactive compensations contribute to improved stability and performance of the MG, especially during sudden load changes or intermittent renewable energy generation. Therefore, the feed-forward term acts as a predictive element, reducing the reliance on corrective feedback actions alone. Subsequently, the overall control system becomes more robust, responsive, and capable of maintaining the desired voltage and frequency levels.

In conventional GFM controls, there is no additional signal for overall voltage improvement; only the voltage of the corresponding bus is considered. For this purpose, the matrix $\boldsymbol{K}$ is incorporated into the voltage control loops in both the d and q axes. In this paper, let $b = 1, \ldots, N_b$ represent the bus counter, where N_b is the total number of buses, and $\{i, n\} \in b$. The variable $\boldsymbol{y}$ denotes the average value across all buses, and it is defined as,

$$\boldsymbol{y}[t+k] = \sum_{b=1}^{N_b} \frac{V_n[t+k]}{N_b}. \tag{27}$$

Referring to (25), let $\boldsymbol{K}[t+k]$ be the designed adaptive controller at time $t+k$. Accordingly, the closed-loop form can be expressed as,

$$\boldsymbol{u}[t+k] = -\boldsymbol{K}[t+k]\boldsymbol{y}[t+k]. \tag{28}$$

Accordingly, the objective in designing the controller is to devise a strategy that effectively utilizes the variable controller $\boldsymbol{K}[t+k]$ to optimize MG performance. This involves formulating a control policy that leverages feedback information to dynamically adjust the controller parameters, ensuring efficient and stable operation of the system. The overarching goal is to meet specified performance criteria, enhance system response, and achieve desired outcomes in the context of the proposed method. An adaptive controller $\boldsymbol{K}[t+k]$, is crucial in MGs with intermittent DERs and the possibility of topology changes due to the dynamic nature of such systems. The need for continuous updates to the adaptive controller arises from two primary factors (i) In MGs, energy generation from RESs like solar and wind can be highly intermittent, leading to variations in power generation. An adaptive controller allows the control system to dynamically adjust to these fluctuations, ensuring optimal performance and stability despite the unpredictable nature of DERs; (ii) MGs may experience changes in their network topology due to various reasons, such as the connection or disconnection of DERs or changes in load distribution. An adaptive controller is essential in adapting the control strategy to accommodate these changes and maintain efficient operation under evolving network configurations. By updating the adaptive controller in real-time based on system conditions and feedback, the control system can effectively respond to the variability in DERs and adapt to changes in the MG's topology. This adaptability is crucial for achieving and maintaining stable and efficient operation in MGs with intermittent DERs and the potential for topology changes. Performance of $\boldsymbol{K}[t+k]$ will be verified in the next section.

IV. RESULTS AND DISCUSSION

A. TEST MG WITH DERS AND RESS

Fig. 3 shows the test system with DERs and RESs, where ω is the angular frequency in rad/s, C_f and L_f are the capacitance and inductance, respectively. It consists of three MGs, i.e., MG1, MG2, and MG3. In MG1, there are two distributed loads with capacities of 25 kVA and 20 kVA. The generation sources in MG1 include a photovoltaic (PV) system with a capacity of 5 kVA, a wind generator (WG) with

TABLE 1. Test MG parameters.

MG 1	Capacity	Converter rate	R_{fil}	L_{fil}	C_{fil}	H_{ini}
CPP	50 kVA	-	0.2 Ω	0.125 mH	0.0025 mF	0.05 GVA·s
DER1	5 kVA	1 kVA	0.05 Ω	0.05 mH	0.001 mF	-
DER2	15 kVA	3 kVA	0.05 Ω	0.05 mH	0.001 mF	-
Load1	25 kVA	5 kVA	0.05 Ω	0.05 mH	0.001 mF	-
Load2	20 kVA	4 kVA	0.05 Ω	0.05 mH	0.001 mF	-
MG 2	Capacity	Converter rate	R_{fil}	L_{fil}	C_{fil}	H_{ini}
CPP	20 kVA	-	0.2 Ω	0.125 mH	0.002 mF	0.03 GVA·s
DER1	3.5 kVA	0.2 kVA	0.05 Ω	0.05 mH	0.001 mF	-
DER2	10 kVA	2 kVA	0.05 Ω	0.05 mH	0.001 mF	-
Load1	22.5 kVA	4.5 kVA	0.05 Ω	0.05 mH	0.001 mF	-
Load2	12 kVA	3 kVA	0.05 Ω	0.05 mH	0.001 mF	-
MG 3	Capacity	Converter rate	R_{fil}	L_{fil}	C_{fil}	H_{ini}
CPP	15 kVA	-	0.2 Ω	0.125 mH	0.002 mF	0.025 GVA·s
DER1	5.5 kVA	1.1 kVA	0.05 Ω	0.05 mH	0.001 mF	-
DER2	5.5 kVA	1.1 kVA	0.05 Ω	0.05 mH	0.001 mF	-
Load1	12.5 kVA	2.5 kVA	0.05 Ω	0.05 mH	0.001 mF	-
Load2	12.5 kVA	2.5 kVA	0.05 Ω	0.05 mH	0.001 mF	-
Utility grid	Capacity	Converter rate	R_{fil}	L_{fil}	C_{fil}	H_{ini}
CPP	200 kVA	-	-	-	-	0.25 GVA·s

a capacity of 15 kVA, and a conventional power plant (CPP) represented by a synchronous generator with a capacity of 50 kVA. In MG2, there are also two distributed loads with capacities of 22.5 kVA and 12 kVA. The generation sources in MG2 consist of a PV system with a capacity of 3.5 kVA, a WG with a capacity of 10 kVA, and a synchronous generator with a capacity of 20 kVA. In MG3, there are two distributed loads, each with a capacity of 25 kVA. The generation sources in MG3 comprise a PV system with a capacity of 5.5 kVA, a WG with a capacity of 5.5 kVA, and a synchronous generator with a capacity of 15 kVA. Other MG's parameters are given in Table 1, where R_{fil}, L_{fil}, C_{fil} are respectively the filtered resistance, inductance, and capacitance, and H_{ini} is the inertial inertia at the normal operating point. All MGs are interconnected. MG1 is linked to MG2 via a circuit breaker, and MG2 is connected to both MG3 and the utility grid, with a total capacity of 200 kVA. To validate our concept, the primary DER in each MG is equipped with a GFM converter modelled as a voltage source converter, while the remaining DERs are connected to the MG using grid-following (GFL) converters modelled as current source converters. To reduce computational demands, all models adopt an average model that neglects the impact of switching and power electronics converters with response times faster than 1 ms. The test system is implemented in MATLAB/Simulink, and the controller $\boldsymbol{K}$ is automatically designed using our modified m-file scripts. All simulations are executed on a high-performance computer featuring a Core i5-12400, 4.2 GHz processor, and 32 GB of RAM. Note that exact MG parameters in Fig. 3 may be withheld due to proprietary information, protecting competitive advantages and security. Assumptions are made to present statistical

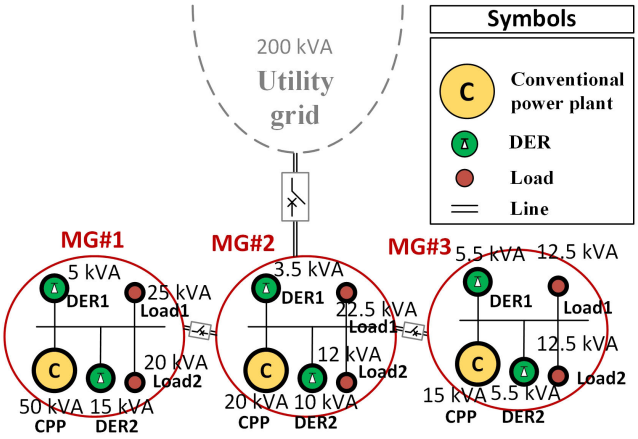

FIGURE 3. Test MG with DERs and RESs.

information while maintaining confidentiality. Accordingly, we have made reasonable assumptions regarding the system parameters to derive the statistical information presented in this study.

To ensure the model accuracy of the proposed data-driven approach based on 4*SID*, the design process of the method meticulously takes into account the accuracy of the model, considering the intermittent nature of DERs and loads. Under these uncertainties, the 4*SID* method is employed to estimate the system model, denoted as $\hat{G}[t+k]$, with a stringent criterion ensuring an accuracy surpassing 85%, $\forall k$. Additionally, we incorporate the consideration of the Hankel singular value, used as a metric to demonstrate how the reduced estimated model captures essential features of the original mode. During simulation, the Hankel singular value

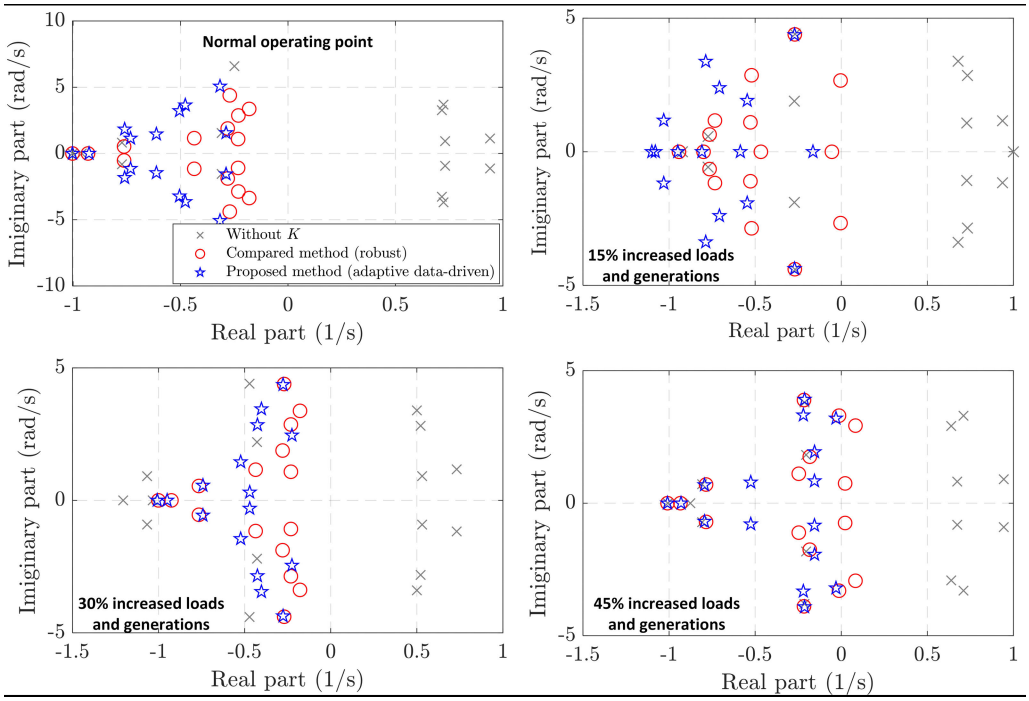

FIGURE 4. Eigenvalue analysis at different operating points.

is set to be lower than 10^{-9} to guarantee that the estimated $\hat{G}[t+k]$ exhibits high accuracy with a concise model order, preserving key features of the dominant oscillation modes.

Following this, the controller introduced in Section III-B is denoted as the "Proposed method". This method is contrasted with two other control strategies: one without an additional controller $\boldsymbol{K}$ in the GFM voltage control loops (denoted by Without $\boldsymbol{K}$) and a conventional robust controller, referred to as the "Compared method". The Compared method is designed based on the normal operating point with fixed control parameters using mixed $\mathcal{H}_2/\mathcal{H}_\infty$-based linear matrix inequality [27]. To achieve this goal, the structure of matrix $\boldsymbol{K}$ is similar to the Proposed method as formulated in (26). The Compared controller aims to minimize the sum of the 2-norm and ∞-norm of matrices $T_2(s) = |\boldsymbol{y}(s) - \boldsymbol{y}^{\text{ref}}|$ and $T_\infty(s) = (I + \hat{G}(s)\boldsymbol{K}(s))^{-1}$. This is expressed as $\min(\gamma_2||T_2(s)||_2 + \gamma_\infty||T_\infty)(s)||_\infty$, with equal weights $\gamma_2 = 1$ and $\gamma_\infty = 1$. Here, the matrix $\hat{G}(s)$ can be obtained from equation (21). In this regard, $\boldsymbol{y}^{\text{ref}}$ represents the vectors of reference signals of $\boldsymbol{y}$, operators $||\cdot||_2$ and $||\cdot||_\infty$ return the 2-norm and ∞-norm of their vector arguments. However, due to the Compared controller's inability to adapt parameters to the MG operating point, optimal parameters are determined using a normal MG operating point.

B. EIGENVALUE ANALYSIS AT FOUR CRITICAL OPERATING POINTS

The small-signal stability analysis with eigenvalue loci at various operating points is essential for ensuring the reliability, robustness, and optimal performance of control systems across a range of operating conditions. As a result, Fig. 4 illustrates the variation in eigenvalues as the operating point changes. In the figure, we assess the performance of the Proposed Method at four distinct operating points: the normal operating point, along with load and generation increases of 15%, 30%, and 45%, while concurrently altering the inertia by -5%, -10%, and -20% relative to the normal operating point.

At the normal operating point, four unstable modes are observable without the presence of a controller. Significantly, both the Compared method and the Proposed method contribute to the enhancement of these unstable modes. In the context of a scenario involving a simultaneous 15% increase in loads and generation, unstable modes also emerge in the absence of a controller. Specifically, in the case of the Compared method, a critical eigenvalue appears at a frequency around 2.5 rad/s. In contrast, no unstable eigenvalues are detected in the case of the Proposed method. The same trends persist when both the loads and generations are increased by 30% and 45%.

This analysis guarantees the effectiveness of the Proposed Method in enhancing system stability compared to the Compared Method, particularly in scenarios with increased loads and generation. The proposed method consistently demonstrates superior performance by preventing the emergence of unstable modes observed in the compared approach. This information is invaluable for ensuring the reliability, robustness, and optimal functioning of control systems across diverse operating conditions.

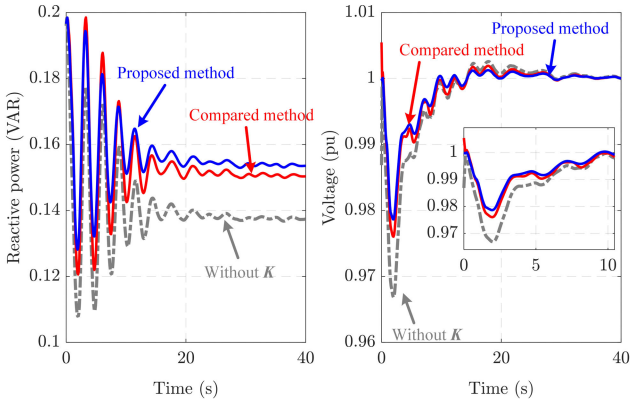

FIGURE 5. Transient responses of average reactive power and voltage of Scenario 1.

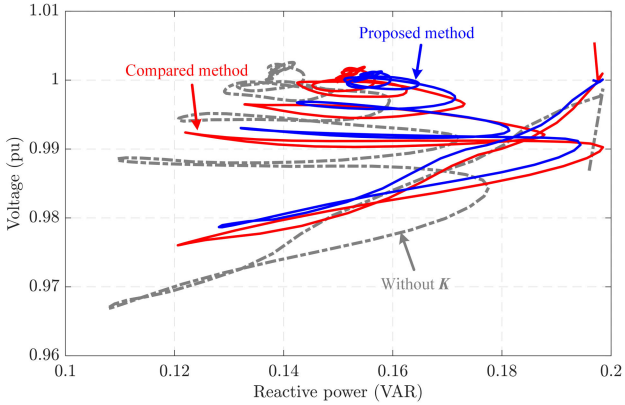

FIGURE 6. Average voltage vs. average reactive power of Scenario 1.

C. PERFORMANCE OF PROPOSED METHOD IN TIME-DOMAIN SIMULATIONS

Time-domain simulations in MGs with DERs serve as a crucial tool to verify and validate proposed control method. The simulations offer a comprehensive insight into the dynamic behavior, stability, and performance of the system across various operating scenarios. Here, we conduct the time-domain simulations including multiple scenarios for a thorough assessment. To assess the efficacy of the proposed adaptive data-driven method, two pivotal scenarios, namely Scenario 1 and Scenario 2, are employed for verification.

In Scenario 1, the MG operates at its normal operating point and grid-connected mode. Periodically, every 1-5 seconds, fluctuations are assumed to occur in the DERs and RES, with deviations of ±20% from their normal active and reactive power outputs, mirroring similar fluctuations in loads. Additionally, at $t = 0.1$ s, the MG is disconnected from the main grid, followed by opening the circuit breaker between MG 2 and the utility grid. As a result, Fig. 5 illustrates the transient responses of the average reactive power and voltage across all buses in the specified case study. As can be seen, the reactive power in the case of without $\boldsymbol{K}$ is low and cannot be recovered when the MG is subjected to disturbance of line tripping and uncertainties from intermittent RESs and DERs. Moreover, Fig. 6 depicts a graphical representation of the interrelationships between average voltage and reactive power. Obviously, the absence of controller $\boldsymbol{K}$ leads to more pronounced fluctuations in reactive power and voltage. This, in turn, results in a larger boundary for reactive power and voltage when the system is subjected to disturbances and intermittency. On the other hand, the boundaries of average reactive power and voltage are constrained by both the Compared method and the Proposed method. Nevertheless, the Proposed method exhibits a slightly superior response.

In Scenario 2, the MG operates exclusively in islanding mode, with MG 2 disconnected from the utility grid. This configuration results in a significantly low inertia MG. All conditions remain consistent with those in Scenario 1, except for an simultaneous increase of 50% in both loads and

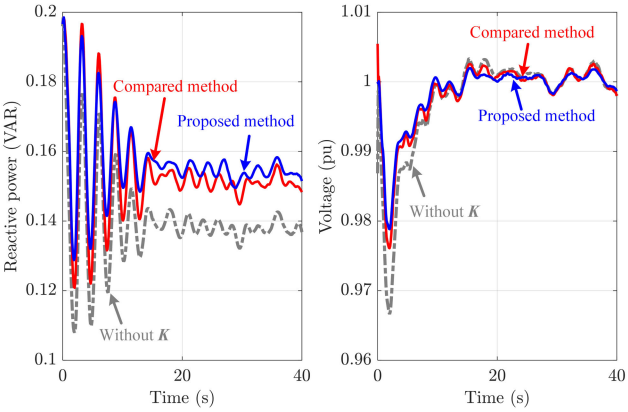

FIGURE 7. Transient responses of average reactive power and voltage of Scenario 2.

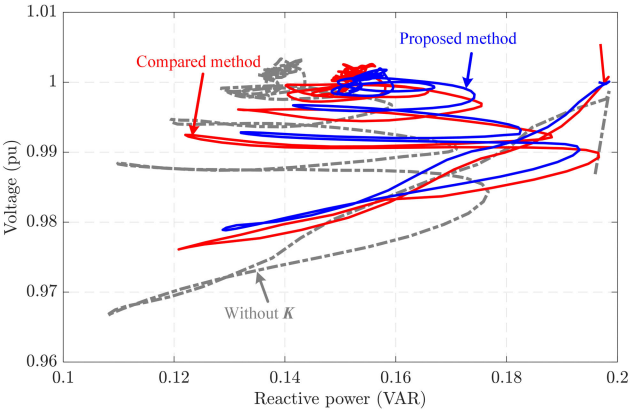

FIGURE 8. Average voltage vs. average reactive power of Scenario 2.

generations compared to Scenario 1. Additionally, the inertia is reduced when the conventional power plant in MG 3 is disconnected from the system at $t = 0.1$ second. Fig. 7 illustrates the reactive power and voltage responses in this scenario. As observed, in the absence of a controller, the voltage experiences a rapid decline in the initial phase of disconnection. Nevertheless, the adverse effects are mitigated when employing both the Compared method and the Proposed method, with the latter demonstrating a more effective response in reducing the impact. The correlation

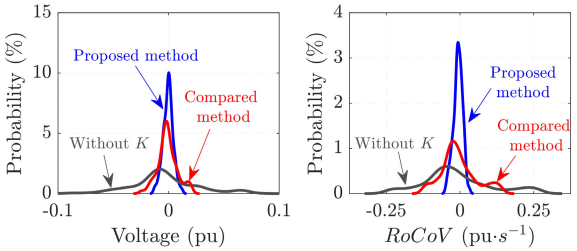

FIGURE 9. Probabilistic analysis under different fault conditions.

between average reactive power and voltage depicted in Fig. 8 follows a similar trend to that observed in Scenario 1, reaffirming that the Proposed method provides the most effective solution among the compared methods.

Furthermore, the proposed method undergoes validation across various fault scenarios. This study assumes the occurrence of a random three-phase fault at each bus for a duration of 100 ms, while concurrently modifying the generation and loads within a range of ±50% compared to the preceding investigation. Furthermore, the overall inertia is subject to random variations of ±50% compared to Scenario 1. Here, $T_{window} = 50$ s is set, and subsequently, the maximum values of voltage and RoCoV are gathered. The simulations are iteratively performed for 1,000 scenarios, with changes in fault locations, as well as variations in generation and loading conditions for each simulation. As a result, Fig. 9 illustrates the probabilistic results of voltage and *RoCoV* under distinct fault conditions. It is evident that the proposed method effectively limits the fluctuations in voltage and *RoCoV* to a smaller range when compared to the Compared method and without $\boldsymbol{K}$. These probabilistic results substantiates that the proposed method performs exceptionally well under diverse fault conditions, especially in variable inertia scenarios.

V. CONCLUSION

This paper presents a control technique for adjusting voltage in variable-inertia MGs with RESs and DERs. The technique uses advanced data-driven algorithms to adaptively change control parameters in response to real-time grid conditions. This improves control performance and accommodates the unpredictable nature of RESs. The simulation results show that the technique effectively optimizes voltage control in variable-inertia MGs. This is a big step forward in controlling renewable energy sources and distributed energy resources for stable grids and good power quality in the shift to sustainable energy systems.

The significant findings are summarized as follows: (i) in the eigenvalue analysis, the obtained results highlight the presence of unstable modes in the normal operating point without a controller and demonstrates the impact of both the Compared method and the Proposed method in amplifying these unstable modes. Additionally, it points out the occurrence of unstable modes under increased loads and generation. The comparison between the Compared method and the Proposed method specifically notes a critical eigenvalue in the former at a certain frequency, whereas the latter exhibits stability with no observable unstable eigenvalues. This analysis suggests that the Proposed method can offer improved stability compared to the Compared method under the specified variable inertia, generation, and loading conditions; (ii) in the time-domain simulations, they are conducted in the variable-inertia MG study with DERs provide valuable insights into the system's dynamic behavior, stability, and performance under various operating scenarios. Two key scenarios, Scenario 1 and Scenario 2, were instrumental in verifying the proposed adaptive data-driven method. The proposed adaptive data-driven method exhibited superior performance in controlling reactive power and voltage in both grid-connected and islanding scenarios. This emphasizes its effectiveness in enhancing the stability and resilience of MG operations under diverse conditions. Moreover, the proposed method undergoes validation across diverse fault scenarios. The simulations cover various scenarios that the proposed method effectively limits voltage and *RoCoV* fluctuations in varied conditions.

REFERENCES

[1] A. A. Memon, M. Karimi, and K. Kauhaniemi, "Evaluation of new grid codes for converter-based DERs from the perspective of AC microgrid protection," *IEEE Access*, vol. 10, pp. 127005–127030, 2022.
[2] M. H. Saeed, W. Fangzong, B. A. Kalwar, and S. Iqbal, "A review on microgrids' challenges & perspectives," *IEEE Access*, vol. 9, pp. 166502–166517, 2021.
[3] Y. Zahraoui, I. Alhamrouni, S. Mekhilef, M. R. Basir Khan, M. Seyedmahmoudian, A. Stojcevski, and B. Horan, "Energy management system in microgrids: A comprehensive review," *Sustainability*, vol. 13, no. 19, p. 10492, Sep. 2021.
[4] W. Pinthurat, P. Kongsuk, and B. Marungsri, "Robust-adaptive controllers designed for grid-forming converters ensuring various low-inertia microgrid conditions," *Smart Cities*, vol. 6, no. 5, pp. 2944–2959, Oct. 2023.
[5] P. Khemmook, K. Prompinit, and T. Surinkaew, "Control of a microgrid using robust data-driven-based controllers of distributed electric vehicles," *Electric Power Syst. Res.*, vol. 213, Dec. 2022, Art. no. 108681.
[6] I. Ngamroo and T. Surinkaew, "Control of distributed converter-based resources in a zero-inertia microgrid using robust deep learning neural network," *IEEE Trans. Smart Grid*, vol. 15, no. 1, pp. 49–66, Jan. 2024.
[7] D. E. Ochoa, F. Galarza-Jimenez, F. Wilches-Bernal, D. A. Schoenwald, and J. I. Poveda, "Control systems for low-inertia power grids: A survey on virtual power plants," *IEEE Access*, vol. 11, pp. 20560–20581, 2023.
[8] P. A. Ahangar, S. A. Lone, and N. Gupta, "Combining data-driven and model-driven approaches for optimal distributed control of standalone microgrid," *Sustainability*, vol. 15, no. 16, p. 12286, Aug. 2023.
[9] C. Li, Y. Yang, T. Dragicevic, and F. Blaabjerg, "A new perspective for relating virtual inertia with wideband oscillation of voltage in low-inertia DC microgrid," *IEEE Trans. Ind. Electron.*, vol. 69, no. 7, pp. 7029–7039, Jul. 2022.
[10] C. Zhang, X. Dou, Z. Zhang, G. Lou, F. Yang, and G. Li, "Inertia-enhanced distributed voltage and frequency control of low-inertia microgrids," *IEEE Trans. Power Syst.*, vol. 36, no. 5, pp. 4270–4280, Sep. 2021.
[11] G. Lin, J. Ma, Y. Li, C. Rehtanz, J. Liu, Z. Wang, P. Wang, and F. She, "A virtual inertia and damping control to suppress voltage oscillation in islanded DC microgrid," *IEEE Trans. Energy Convers.*, vol. 36, no. 3, pp. 1711–1721, Sep. 2021.
[12] Z. Lv, Y. Zhang, Y. Xia, and W. Wei, "Adjustable inertia implemented by bidirectional power converter in hybrid AC/DC microgrid," *IET Gener., Transmiss. Distrib.*, vol. 14, no. 17, pp. 3594–3603, Sep. 2020.
[13] Y. Yang, C. Li, J. Xu, F. Blaabjerg, and T. Dragicevic, "Virtual inertia control strategy for improving damping performance of DC microgrid with negative feedback effect," *IEEE J. Emerg. Sel. Topics Power Electron.*, vol. 9, no. 2, pp. 1241–1257, Apr. 2021.

[14] R. Liu, S. Wang, G. Liu, S. Wen, J. Zhang, and Y. Ma, "An improved virtual inertia control strategy for low voltage AC microgrids with hybrid energy storage systems," *Energies*, vol. 15, no. 2, p. 442, Jan. 2022.
[15] S. Bagheri and H. M. CheshmehBeigi, "DC microgrid voltage stability through inertia enhancement using a bidirectional DC–DC converter," in *Proc. 7th Iran Wind Energy Conf. (IWEC)*, May 2021, pp. 1–5.
[16] C. García-Ceballos, S. Pérez-Londoño, and J. Mora-Flórez, "Iterative approach for tuning multiple converter-integrated DER in microgrids," *Int. Trans. Electr. Energy Syst.*, vol. 2022, pp. 1–15, Apr. 2022.
[17] M. Y. Worku, M. A. Hassan, and M. A. Abido, "Power management, voltage control and grid synchronization of microgrids in real time," *Arabian J. Sci. Eng.*, vol. 46, no. 2, pp. 1411–1429, Feb. 2021.
[18] M. Baharizadeh, M. S. Golsorkhi, M. Shahparasti, and M. Savaghebi, "A two-layer control scheme based on P–V droop characteristic for accurate power sharing and voltage regulation in DC microgrids," *IEEE Trans. Smart Grid*, vol. 12, no. 4, pp. 2776–2787, Jul. 2021.
[19] K. S. Ratnam, K. Palanisamy, and G. Yang, "Future low-inertia power systems: Requirements, issues, and solutions—A review," *Renew. Sustain. Energy Rev.*, vol. 124, May 2020, Art. no. 109773.
[20] P. Makolo, R. Zamora, and T.-T. Lie, "The role of inertia for grid flexibility under high penetration of variable renewables—A review of challenges and solutions," *Renew. Sustain. Energy Rev.*, vol. 147, Sep. 2021, Art. no. 111223.
[21] M. Shahbazitabar, H. Abdi, H. Nourianfar, A. Anvari-Moghaddam, B. Mohammadi-Ivatloo, and N. Hatziargyriou, "An introduction to microgrids, concepts, definition, and classifications," *Microgrids: Advances in Operation, Control, and Protection*. New York, NY, USA: Springer, 2021, pp. 3–16.
[22] Z. Wang, F. Zhuo, H. Yi, J. Wu, F. Wang, and Z. Zeng, "Analysis of dynamic frequency performance among voltage-controlled inverters considering virtual inertia interaction in microgrid," *IEEE Trans. Ind. Appl.*, vol. 55, no. 4, pp. 4135–4144, Jul. 2019.
[23] P. Tielens and D. Van Hertem, "The relevance of inertia in power systems," *Renew. Sustain. Energy Rev.*, vol. 55, pp. 999–1009, Mar. 2016.
[24] I. Ngamroo and T. Surinkaew, "Adaptive robust control based on system identification in microgrid considering converter controlled-based generator modes," *IEEE Access*, vol. 9, pp. 125970–125983, 2021.
[25] A. F. El-Hamalawy, M. E. Ammar, H. F. Sindi, M. F. Shaaban, and H. H. Zeineldin, "A subspace identification technique for real-time stability assessment of droop based microgrids," *IEEE Trans. Power Syst.*, vol. 37, no. 4, pp. 2731–2743, Jul. 2022.
[26] R. G. Wilson, D. G. Fisher, and D. E. Seborg, "Model reduction and the design of reduced-order control laws," *AIChE J.*, vol. 20, no. 6, pp. 1131–1140, Nov. 1974.
[27] L. Fortuna, M. Frasca, and A. Buscarino, *Optimal and Robust Control: Advanced Topics With MATLAB*. Boca Raton, FL, USA: CRC Press, 2021.

WATCHARAKORN PINTHURAT (Member, IEEE) received the M.Eng. degree in energy engineering from the Asian Institute of Technology, Bangkok, Thailand, in 2016, and the Ph.D. degree in electrical engineering from the University of New South Wales, Sydney, Australia, in 2023.

Currently, he is a Lecturer with the Department of Electrical Engineering, Rajamangala University of Technology Tawan-Ok, Chanthaburi, Thailand. His current research interests include control of distributed energy storage systems, applications of deep reinforcement learning for distributed energy storage systems, and hybrid energy storage systems.

PRAYAD KONGSUK received the M.Eng. degree from the King Mongkut's University of Technology North Bangkok, in 2003, and the Ph.D. degree from the King Mongkut's Institute of Technology Ladkrabang, Bangkok, Thailand, in 2020, all in electrical engineering.

He is currently an Assistant Professor with the Department of Electrical Engineering, Rajamangala University of Technology Tawan-Ok, Chanthaburi, Thailand. His current research interests include power electronics, motor drives, control systems, and energy management systems.

TOSSAPORN SURINKAEW received the Ph.D. degree in electrical engineering from Central Queensland University, Australia, in 2022.

He is a Lecturer with the School of International and Interdisciplinary Engineering, Faculty of Engineering, King Mongkut's Institute of Technology Ladkrabang, Thailand. His research interests include power system modeling, computation, control, and dynamics, with a particular interest in future grid stability.

BOONRUANG MARUNGSRI (Member, IEEE) was born in Nakhon Ratchasima, Thailand, in 1973. He received the B.Eng. and M.Eng. degrees from Chulalongkorn University, Thailand, in 1996 and 1999, respectively, and the D.Eng. degree from Chubu University, Kasugai, Aichi, Japan, in 2006, all in electrical engineering.

He is an Assistant Professor with the School of Electrical Engineering, Suranaree University of Technology, Thailand. His areas of interests include smart grids, energy systems, and high voltage insulation technologies.